Inventory of Supplementary Materials:

Gene	% SDC positioning	% Spindle misalignment	% Abnormal nuclear shape
Control	0 (n=11)	0 (n=11)	0 (n=11)
spd-3(oj35)	100 (n=11)	55.6 (n=11)	100 (n=11)
ucr-1 RNAi	0 (n=3)	33.3 (n=3)	0 (n=3)
mev-1 RNAi	0 (n=2)	50.0 (n=2)	0 (n=3)
isp-1(qm150)	0 (n=10)	20.0 (n=10)	N.A.
cco-1 RNAi	0 (n=5)	40.0 (n=5)	0 (n=3)
clk-1(qm30)	0 (n=10)	0 (n=10)	N.A.

Table S1. Strains and RNAi feeding clones for the electron transfer chain (ETC) pathway and sorting and assembly machinery (SAM) complex in mitochondria, related to Figure 1.

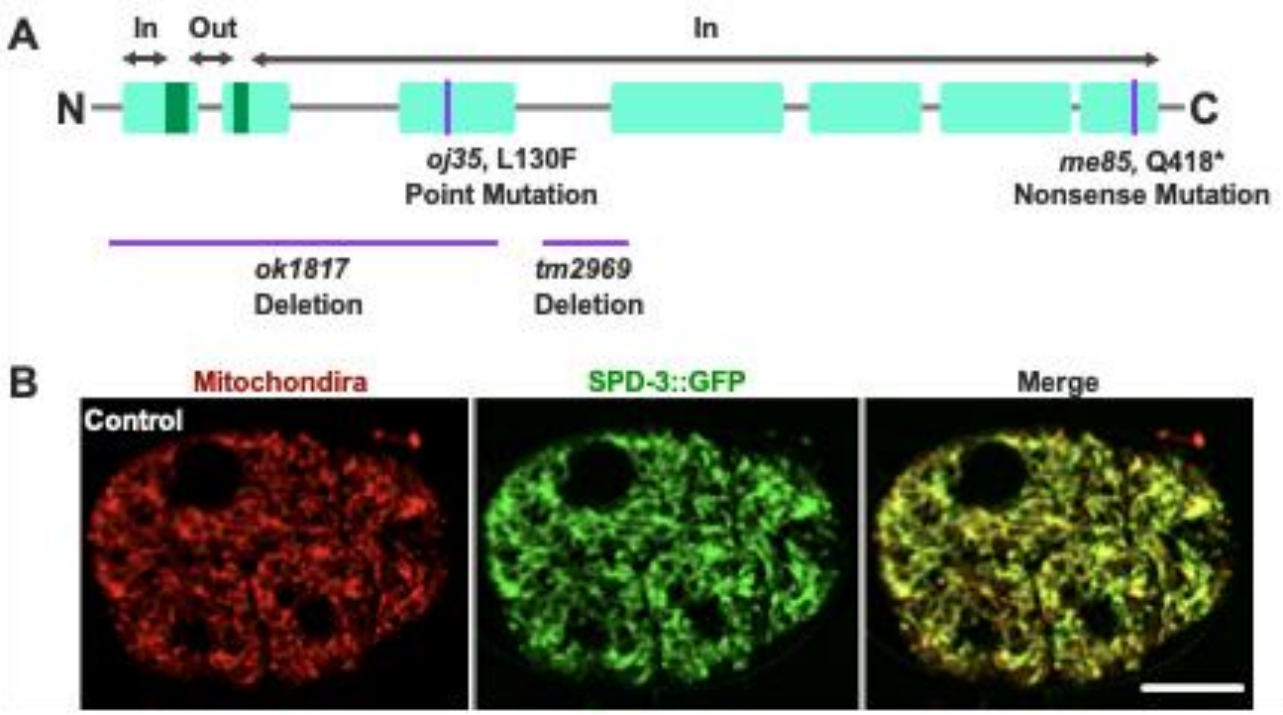

Figure S1. SPD-3 localizes to mitochondria, related to Figure 1. (**A**) Diagram of the *spd-3* gene indicating the position of the *oj35* and *me85* mutation, and two deletion alleles, *ok1817* and *tm2929*. (**B**) SPD-3::GFP colocalizes with mitochondria stained by the mitochondrial dye MitoTracker CMXRosetta. Scale bar, 10 μm.

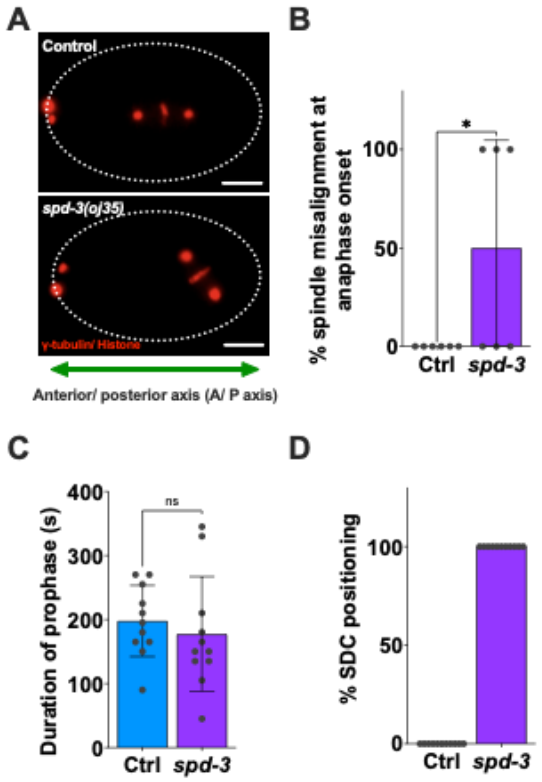

Figure S2. *spd-3(oj35)* is defective in mitotic spindle alignment and chromosome positioning, related to Figure 1. (**A**) Images of embryos coexpressing mCherry::histone H2B and mCherry::γ-tubulin in control (**top**, Ctrl) and *spd-3(oj35)* (**bottom**, *spd-3*). In control embryos, the mitotic spindle is aligned along the anterior/posterior axis (A/P axis). The mitotic spindle failed to misalign to the A/P axis in *spd-3(j35)* embryos. Scale bars, 10 μm. (**B**) Plot of the percentage of spindle misalignment in control (n=11) and *spd-3(oj35)* (n=11) embryos at anaphase onset. (**C**) Plot of the duration of mitotic prophase. Duration of prophase is defined by the time between pronuclei meeting and NEBD (n=11 embryos for control and *spd-3*). Error bars are SD. The significance of the difference between strains was determined by t-tests. ns indicates no significant difference. (**D**) Graph plotting the percentage of socially distanced chromosomes during mitosis (n>11 embryos for control and *spd-3*).

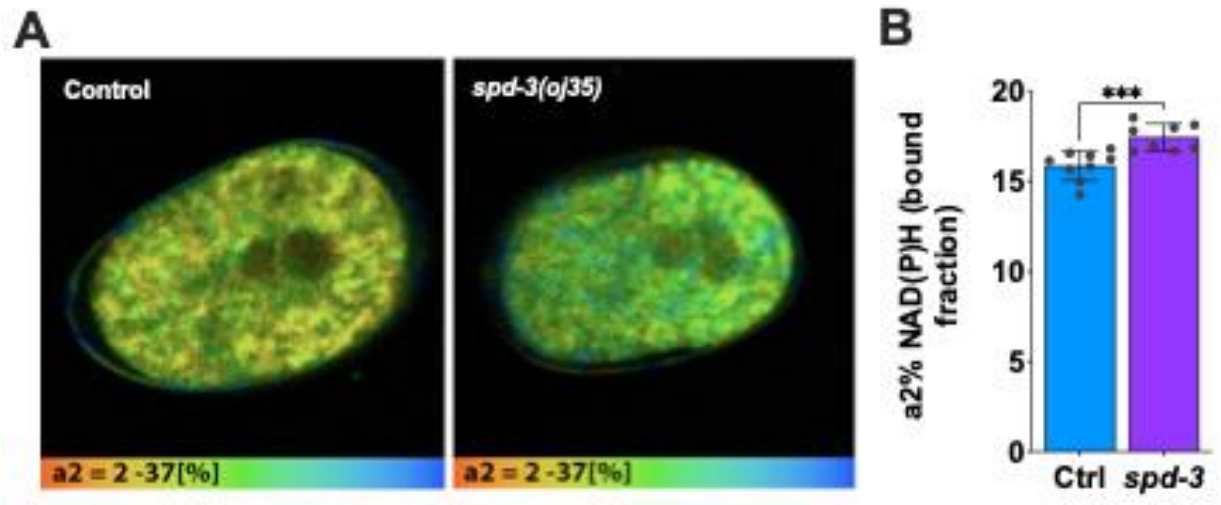

Figure S3. FLIM NAD(P)H imaging shows increased metabolic rates in *spd-3(oj35)* embryos, related to Figure 1. (**A**) Images showing color-coded values of NAD(P)H bound fraction in control (Ctrl) and *spd-3(oj35)* (*spd-3*) one cell stage *C. elegans* embryo. Bottom gradient indicates the level of bound NAD(P)H reaching from 2-37%. (**B**) Bar chart graph comparing mean values for NAD(P)H bound fraction (a2%) in tested embryos. Mean pixel value was calculated from 2-3 image acquisitions per embryo. n=9 for control and n=8 for *spd-3(oj35).*

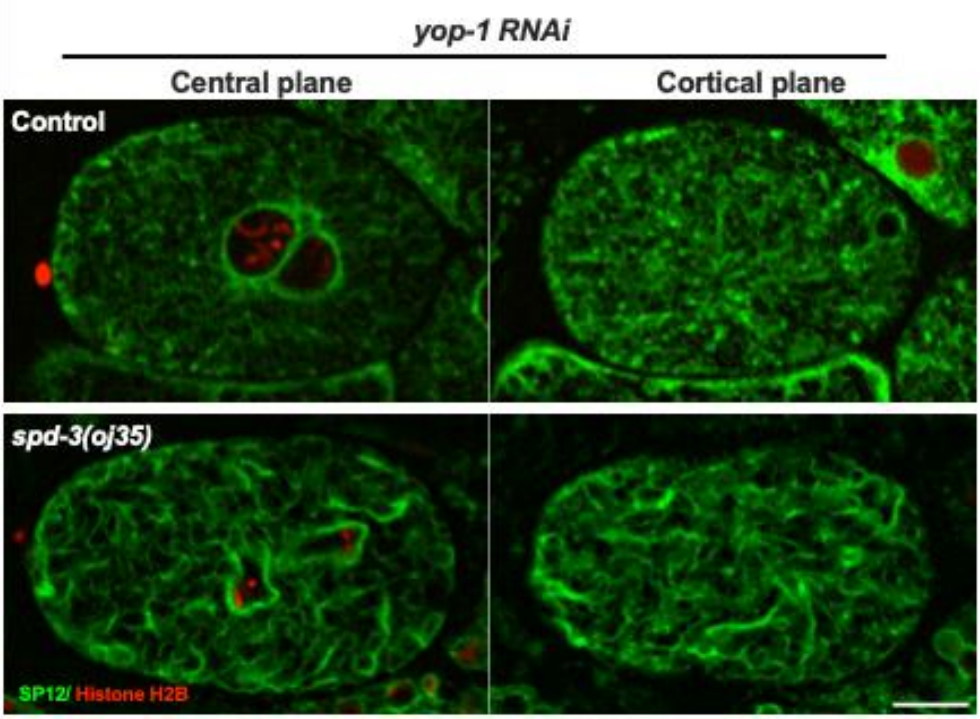

Figure S4. Socially distanced chromosome positioning is not rescued by the removal of ER clusters, related to Figure 2. Spinning-disk confocal images of embryos in control (**top**) and *spd-3(oj35)* (**bottom**) with *yop-1 (RNAi)*. Representative images of a central (**left**) and cortical plane (**right**) are shown. Embryos express the GFP-tagged ER marker SP12 and histone H2B labeled with mCherry. Scale bar, 10 μm.

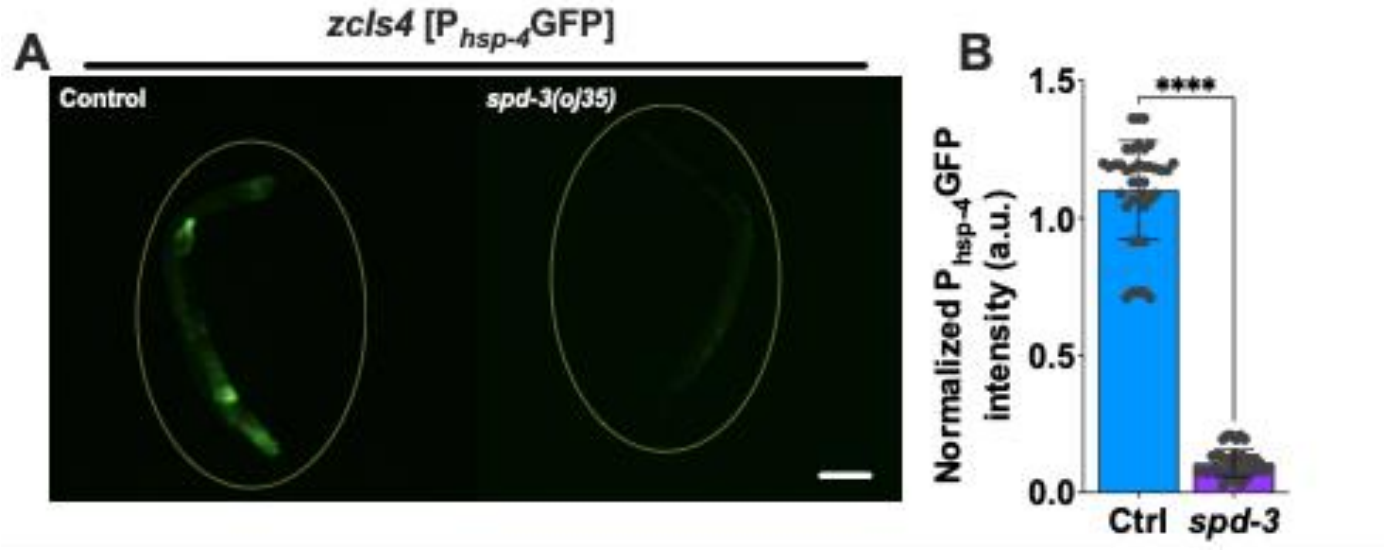

Figure S5. Reduction of *hsp-4::gfp* in *spd-3(oj35)* adult animals, related to Figure 2. (**A**) Fluorescence images of control (Ctrl) and *spd-3(oj35)* (*spd-3*) adult animals carrying the P*hsp-4*::GFP (*zcIs4*) transgene. Scale bar, 100 μm. (**B**) Graph plotting the normalized overall fluorescence of *zcIs4* in control (n=40) and *spd-3(oj35)* (n=40). Error bars are SD. The significance of the difference between strains was determined by t-tests. ****P<0.0001.

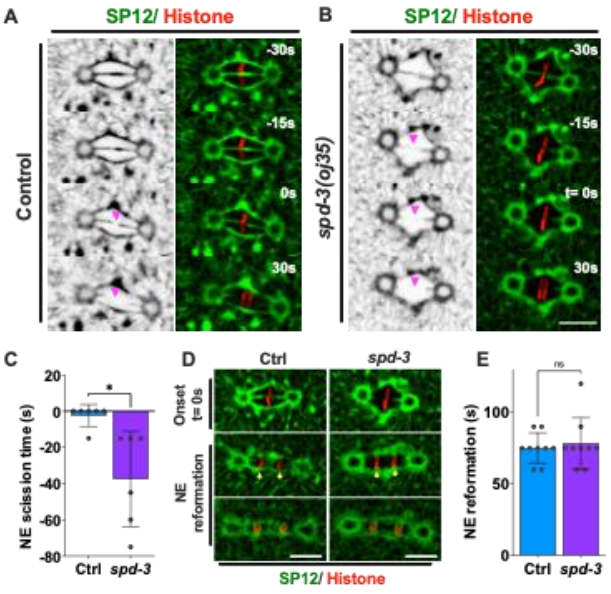

Figure S6. SPD-3 is required for nuclear envelope disassembly and assembly, related to Figure 2. (**A, B**) Fluorescence confocal images of control (Ctrl) and *spd-3(oj35) (spd-3)* embryos expressing GFP::SP12 and mCherry::histone H2B. The left panel shows SP12 alone, the right panel shows a merge of SP12 and Histone. Magenta arrowheads mark the site of nuclear envelope scission in control (**A**) and *spd-3(oj35)* (**B**). (**C**) Graph plotting time of nuclear envelope scission in control (**left**, n=7) and *spd-3(oj35)* (**right**, n=7). (**D**) Fluorescence confocal images of control and *spd-3(oj35)* embryos expressing GFP::SP12 and mCherry::histone H2B. Yellow arrowheads mark the site of nuclear envelope reformation in control (**top**) and *spd-3(oj35)* (**bottom**). (**E**) Graph plotting time of nuclear envelope reformation in control (left, n=9) and *spd-3(oj35)* (right, n=9). (**A, B, D**) Scale bars, 10 μm. (**A-E**) Times are in seconds relative to anaphase onset (t= 0). (**C, E**) Error bars are SD. The significance of the difference between strains was determined by t-tests. ns indicates no significant difference. *P<0.05.

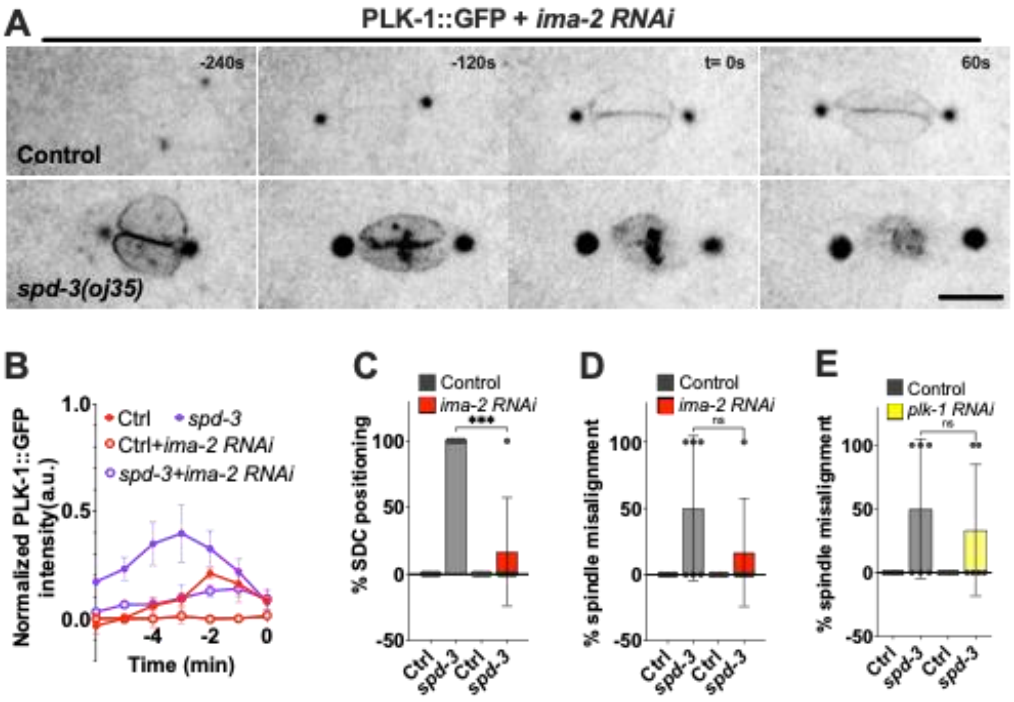

Figure S7. Reduction of PLK-1 in nucleoplasm can prevent the socially distanced chromosome positioning and spindle misalignment, related to Figure 4. (**A**) Time-lapse sequences of embryos expressing GFP::PLK-1 in control (Ctrl) and *spd-3(oj35)* (*spd-3*) exposed to *ima-2* (*RNAi)*. Times are in seconds relative to anaphase onset (t= 0). Scale bars, 10 µm. (**B**) Quantitation of normalized PLK-1::GFP intensity in the nucleoplasm of embryos from time-lapse sequences as in *(A)*. The value of PLK-1 intensity in control (red, n=3 for each condition) and *spd-3(oj35)* (purple, n=3 for each condition) without (solid) and with (empty) *ima-2 (RNAi)*. Error bars are SD. (**C-E**) Graph plotting percentage of SDC (**C**) and spindle misalignment (**D, E**) in control and *spd-3(oj35)*. *ima-2 RNAi* is in red (n=3 for each strain), and *plk-1 RNAi* (n=6 for each strain) is in yellow.

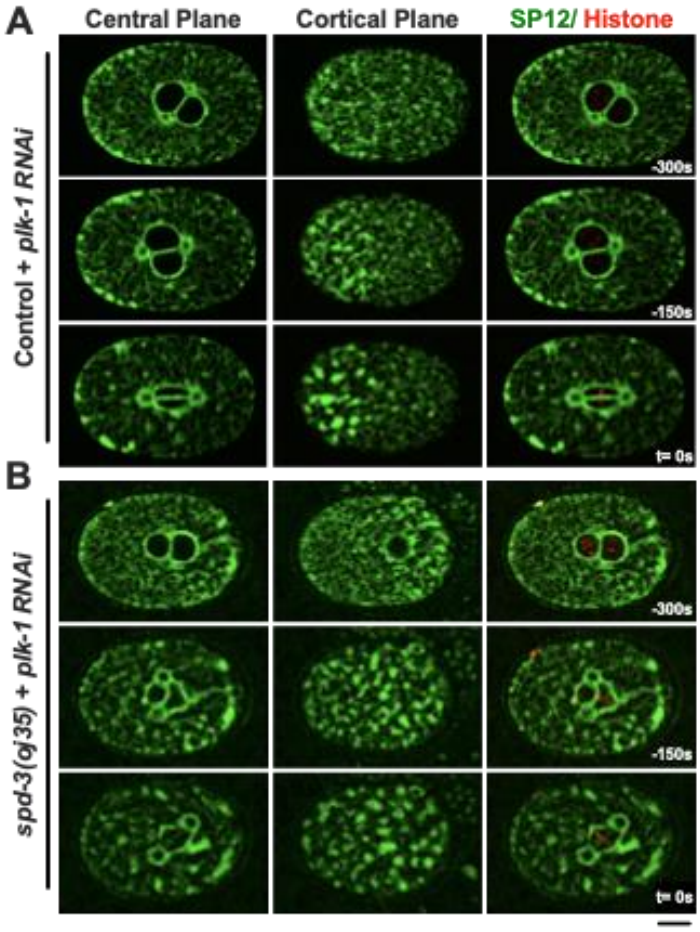

Figure S8. Changes in ER morphology are not induced by elevated PLK-1 levels, related to Figure 5. (**A**) Representative images of control embryos treated with *plk-1* (*RNAi*) coexpressing SP12::GFP and mCherry::histone H2B. Images of the ER marker SP12 acquired at the central (**left**) and cortical plane (**middle**) and a merge of SP12 and histone H2B (**right**) are shown. (**B**) The same layout of images as in (**A**) but showing the morphology of ER after *plk-1* (RNAi) in the *spd-3(oj35)*. Times are in seconds relative to anaphase onset (t= 0). Scale bars, 10 μm.

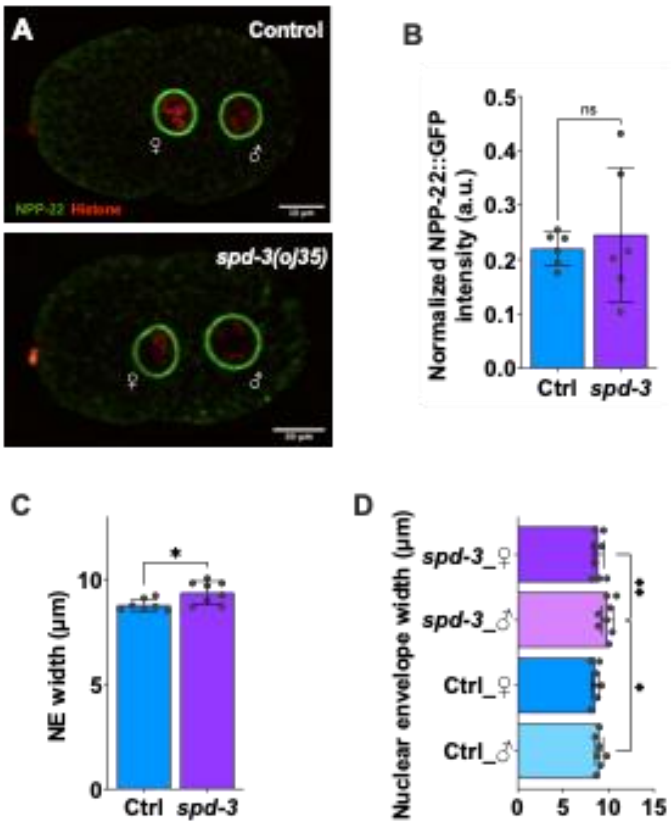

Figure S9. The male pronucleus expands before the pronuclear meeting, related to Figure 5. (**A**) Representative images of embryos coexpressing NPP-22::mNG and mCherry::histone H2B in control (Ctrl) and *spd-3(oj35)* (*spd-3*). Scale bars, 10 μm. (**B**) Plot the intensity of NPP-22::mNG in the nuclear membrane of control (n=7) and *spd-3(oj35)* (n=8). (**C**) Plot of the pronuclear envelope width in control and *spd-3(oj35).* (**D**) Plot the nuclear envelope width of male and female pronuclei in control and *spd-3(oj35).* (**B-D**) Error bars are SD. The significance of the difference between strains was determined by t-tests. ns indicates no significant difference. *P<0.05. **P<0.01.

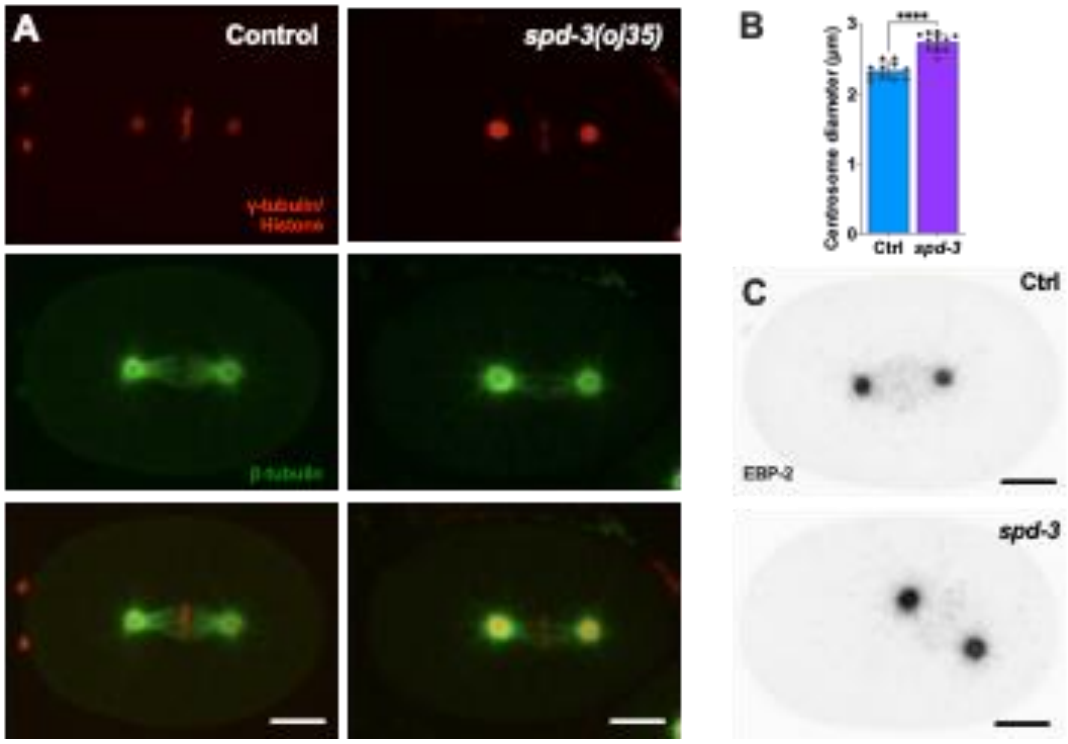

Figure S10. The pericentriolar material increases in size in *spd-3(oj35),* related to Figure 5. (A) Spinning-disk confocal images of embryos in control (**left**, Ctrl) and *spd-3(oj35)* (**right**, *spd-3*). Embryos are coexpressing mCherry::γ-tubulin, mCherry::histone H2B, and GFP::β-tubulin. (**B**) Plots of the centrosome size in control (n=11) and *spd-3(oj35)* (n=11). The diameter of centrosomes was measured by the intensity of mCherry::γ-tubulin. (**C**) Spinning-disk confocal images of embryos in control (**left**, Ctrl) and *spd-3(oj35)* (**right**, *spd-3*). Embryos are coexpressing mCherry::histone H2B, and EBP-2::GFP. (**A, C**) Scale bars, 10 μm.

SUPPLEMENTAL MATERIALS AND METHODS

C. elegans strains used in this study

Strain	Genotype
N2 (Bristol)	Wild-type (ancestral)
SA250	*unc-119(ed3) III; tjIs54* [P_{pie-1}GFP::TBB-2 + P_{pie-1}2xmCherry::TBG-1 + *unc-119(+)*]*; tjIs57* [P_{pie-1}mCherry::HIS-48 + *unc-119(+)*]
WH327	*unc-119(ed3) III; ojIs23* [P_{pie-1}GFP::SP12]
SBW244	*sbw8* [*ndc1(npp-22)::mNeoGreen*]
UV117	*jf98* [*gfp::lmn-1*] I
OD2425	*lt18* [*plk-1::sgfp*]*::loxp* III
WH342	*unc-119(ed3) III; ojIs31* [P_{pie-1}SPD-3::GFP + *unc-119(+)*]
SJ4005	*zcIs4* [P_{hsp-4}GFP]
TV24458	*wow47* [*ebp-2::gfp::3xflag)*] *II; zif-1(gk117) III; wyEx9745*

The *C. elegans* strains used in this study are listed in the table above. The *spd-3(oj35)* allele was outcrossed against N2 five times before crossing into fluorescent marker strains for phenotypic analysis.

C. elegans strains and alleles:

The Bristol strain N2 was used as the standard wild-type strain. Culturing, handling, and genetic manipulation of *C. elegans* were performed using standard procedures (Brenner 1974). All *C. elegans* strains and the temperature-sensitive strain *spd-3(oj35)* were maintained at 16°C and L4 hermaphrodites were shifted to room temperature (~23°C) overnight and heat-shocked at 25°C for 4 hr prior to analysis. The following alleles and strains were used: LGIII: *clk-1(qm30);* LGIV: *isp-1(qm150), spd-3(oj35)*. They were backcrossed four times with wild-type animals before being used for genetic analyses.

C. elegans RNA-mediated interference

Primers for *C. elegans* RNAi feeding clones

Gene	Primer 1	Primer 2	Template
F26B1.3 *(ima-2)*	TATAGCGGCCGCCTGTC TCACAATGCCGAAGA	ATAGCTAGCTGTCAGC GAGTCATTTCCAG	N2 genomic
C14B9.4 *(plk-1)*	TATAGCGGCCGCTCAAC AACAAGCTGCAGAGG	ATAACGCGTTGGGACTA AAAGGGTCGATG	N2 genomic

RNA-mediated interference:

The *ucr-1, mev-1, cco-1, mtx-1, gop-3, yop-1, hsp-3, hsp-4, ima-2* and *plk-1* (RNAi) were administered by feeding. Feeding vector (L4440) was obtained from the Addgene. The *ima-2 and plk-1* (RNAi) feeding vectors were constructed by cloning the *ima-2* and *plk-1* genomic DNA into the L4440 feeding vector, followed by transformation into *Escherichia coli HT115(DE3)* bacteria. The *E. coli HT115(DE3)* bacteria containing the feeding vectors were cultured and used to seed RNAi plates (1 mM IPTG and 50 µg/ml ampicillin). L4 hermaphrodites were allowed to feed for 24, or 48 hr at room temperature (~23°C) and then shift to 25°C for 4 hr before analysis. For *plk-1* RNAi, L4 larvae were cultured at room temperature overnight and then transferred to *plk-1* RNAi feeding plates allowed to feed for 6 hr at 25°C before analysis.

Live imaging

Embryos for live-imaging experiments were obtained by dissecting gravid adult hermaphrodites in M9 buffer (42 mM Na_2HPO4, 22 mM KH_2PO_4, 86 mM NaCl, and 1 mM $MgSO_4$). One-cell embryos were mounted on slides with 2% agarose pad, overlaid with a 22 × 22-mm coverslip, and imaged at room temperature on fluorescence microscope (ECLIPSE Ti2; Nikon) equipped with a CFI Apo TIRF 60× 1.45 NA oil immersion lens and a CCD camera (iXon 897 Ultra EMCCDs) or on a 3i VIVO spinning-disc confocal microscope (Axio Examiner.Z1; Zeiss) equipped with Zeiss Plan-Apochromat 63x/1.40 oil microscope objective, 6 laster lines and a Hamamatsu ORCA-Flash4.0 scientific CMOS camera (Hamamatsu) for detection. For z-stacks, images in a 27-micron z-series (1 micron per section) were captured every 15 s (Figure 1A, B, D, E; Table S1; Fig. S2; Fig. S5; Fig. S10A). The microscope was controlled by Nikon NIS-Elements software (Nikon). Fluorescence confocal images were acquired every 10 s (Figure 4, 5; Fig. S8; Fig. S9) or 15 s (Figure 1-3; Fig. S4; Fig. S6; Fig. S7) by collecting 31 z-planes at 1.0-µm intervals or 17 z-planes at 1-µm intervals without binning. Imaging was initiated in one-cell embryos before pronuclear meeting and was terminated 3 min after anaphase onset. EBP-2::GFP images acquired at 400 msec intervals and each movie was 150 frames per 1 min (Fig. S10C). Acquisition parameters were controlled using a Slidebook 6.0 program (3i - Intelligent Imaging).

Image analysis

All images were processed and analyzed using ImageJ (National Institutes of Health). For figure construction, final image panels were scaled for presentation in Prism v9.5.0 (GraphPad). Lamin fluorescence intensity (GFP::LMN-1) was quantified using ImageJ software by drawing a box around the nuclei and subtracting the background fluorescence in an equal-sized box drawn over the cytoplasm (Fig 3C and D). To quantify the PLK-1::GFP fluorescence in nucleoplasm, a fixed-size box was drawn in nucleoplasm (red box) and in cytoplasm (black box) as background at each time point. The normalized PLK-1 level was calculated as [(integrated intensity in red box – integrated intensity in black box)/ integrated intensity in black box] (Fig. 4C and D; Fig. S7B). A gamma of 1.5 was applied for images of centrosomal PLK-1::GFP (Fig. 4E) to visualize centrioles in the mutants, while not oversaturating the signal in the WT centrosomes. The fluorescence of *hsp-4::ghp* reporter was measured using ImageJ software by drawing a box around the individual worm for quantification and subtracting the background fluorescence in an equal-sized box drawn over the background fluorescence (Fig. S5). For centrosome size, centrosome was marked with mCherry::γ-tubulin and line scans from single confocal planes over centrosome regions, allowing quantification of the centrosomes diameter and the full width at half maximum taken as centrosome diameter (Fig. S10).

Fluorescence lifetime imaging (FLIM) microscopy

A Zeiss LSM-780 NLO confocal/multiphoton microscopy system consisting of an inverted Axio Observer (Zeiss) microscope, motorized stage for automated scanning, Chameleon Vision-II (Coherent Inc.) ultrafast Ti:sapphire laser with dispersion compensation to maintain pulses at the specimen plane (690– 1,060 nm, 80 MHz, 150 fs) for multiphoton excitation and a standard set of dry and immersion objectives was used. Three HPM- 100-40 hybrid GaAsP detectors (Becker and Hickl) are connected to the nondescanned (NDD) port of the microscope using two T-adapters (Zeiss) with proper dichroics and band pass filters to collect as much fluorescence as possible in the spectral ranges tryptophan channel: 740 nm Ex, 340–380 nm Em, NAD(P)H channel: 740 nm Ex, 460–500 nm Em and FAD channel: 890 nm Ex, 520–560 nm Em. The three channels also contain a 690 nm short pass filter (Zeiss) in the beam path to avoid excitation background. Three SPC-150 cards (Becker and Hickl) synchronized with the pulsed laser and the Zeiss LSM- 780 scan head signals collect the time-resolved fluorescence in TCSPC mode using SPCM (Version 9.74) acquisition software. A motorized stage is used during imaging using Zeiss 40x NA1.3 oil apochromatic objective lens.

FLIM Processing and Analysis

FLIM data fitting is based on the B&H handbook. We used a two components incomplete model to fit Tryptophan, NAD(P)H and FAD/FMN FLIM images. The offset and scattering are set to 0. Shift is optimized to make sure the Chi2 as close as to 1.

The FLIM processing followed the previously published paper (Wallrabe et al. 2018; Cao et al. 2019) with an important advance in normalization of photon reference images to compensate

for varying intensities (FIJI, Plugins -> Integral Image Filters -> Normalize Local Contrast): followed by zero'ing the nucleus; cell segmentation and creating single pixel ROIs by a ImageJ/FIJI custom plugin. The purpose of this sequence is to create pixel locations by X-Y coordinates, specific for embryos. Those locations are then applied to the FLIM data to extract any of the FLIM parameters in the data pool. A custom Python code ultimately analyzes different data combinations to produce ratios, means, medians, and histograms, further charted in MS Excel.

Immunoblotting

200 adult worms from each strain were transferred to 30 µl of sample buffer (80.0 mM Tris pH 6.8, 2.0% SDS, 10.0% glycerol, 0.0006% Bromophenol blue, and 5.0% β-mercaptoethanol), subjected to the freeze-thaw treatment three times in liquid nitrogen and water bath and then boiled in a 95℃-heating block for 5 minutes. The samples were loaded on 10% SDS-PAGE, transferred to a polyvinylidene fluoride (PVDF) membrane and subjected to western blot analysis using anti-PLK-1 (1:3,000 dilution, from Monica Gotta lab). Primary antibodies were detected using IRDye® 680RD goat anti-Rabbit IgG secondary antibody (1:5,000 dilution; Abcam) and then probed for α-tubulin using the monoclonal DM1α antibody (1:3,000 dilution; Sigma Aldrich) to examine the expression levels of α-tubulin as a loading control. PLK-1 western blots were quantified with ImageJ (Fig. 4B and Fig. 5B). Antibody signals were detected using the Azure Biosystems c600 and Li-COR Fc Odyssey imaging system.

Statistical analysis

Statistical analysis was conducted using Prism v9.5.0 (GraphPad). P values were determined using unpaired two-tailed t tests assuming equal SD. $P > 0.05$ (ns), $P < 0.05$ (*), $P < 0.01$ (**), $P < 0.001$ (***), and $P < 0.0001$ (****). Data distribution was assumed to be normal, but this was not formally tested.

SUPPLEMENTAL REFERENCES

Brenner S. (1974). The genetics of *Caenorhabditis elegans*. *Genetics* 77: 71-94.

Cao R, Wallrabe H, Siller K, Rehman Alam S, Periasamy A. (2019). Single-cell redox states analyzed by fluorescence lifetime metrics and tryptophan FRET interaction with NAD(P)H: Single-Cell Redox States Analyzed by FLIM. Cytometry *95*: 110–121.

Wallrabe H, Svindrych Z, Alam SR, Siller KH, Wang T, Kashatus D, Hu S, Periasamy A. (2018). Segmented cell analyses to measure redox states of autofluorescent NAD(P)H, FAD & Trp in cancer cells by FLIM. Sci Rep *8*: 79.